Local volume fraction fluctuations in random media

J. Quintanilla[a] and S. Torquato[b]
Princeton Materials Institute and Department of Civil Engineering & Operations Research, Princeton, New Jersey 08544

(Received 16 July 1996; accepted 11 November 1996)

Although the volume fraction is a constant for a statistically homogeneous random medium, on a spatially local level it fluctuates. We study the full distribution of volume fraction within an observation window of finite size for models of random media. A formula due to Lu and Torquato for the standard deviation or ''coarseness'' associated with the *local* volume fraction ξ is extended for the nth moment of ξ for any n. The distribution function F_L of the local volume fraction of five different model microstructures is evaluated using analytical and computer-simulation methods for a wide range of window sizes and overall volume fractions. On the line, we examine a system of fully penetrable rods and a system of totally impenetrable rods formed by random sequential addition (RSA). In the plane, we study RSA totally impenetrable disks and fully penetrable aligned squares. In three dimensions, we study fully penetrable aligned cubes. In the case of fully penetrable rods, we will also simplify and numerically invert a prior analytical result for the Laplace transform of F_L. In all of these models, we show that, for sufficiently large window sizes, F_L can be reasonably approximated by the normal distribution. © *1997 American Institute of Physics.* [S0021-9606(97)50407-7]

I. INTRODUCTION

The quantitative characterization of the microstructure of random heterogeneous media, such as composite materials, colloidal dispersions, porous media and cracked solids, is crucial in determining the macroscopic physical properties of such materials.[1–5] One of the most important morphological descriptors is the volume fraction of the phases, which, in the case of porous media, is just the porosity (i.e., the volume fraction of the fluid phase). The volume fraction of two-phase random media fluctuates on a spatially local level, even for statistically homogeneous media. A quantitative understanding of how the volume fraction fluctuates locally is of relevance to a number of problems, including scattering by heterogeneous media,[6] transport through composites and porous media,[7] the study of noise and granularity of photographic images,[8–10] the properties of organic coatings,[11] and the fracture of composite materials.[12]

Lu and Torquato[13] represented and computed the standard deviation of the *local volume fraction* $\xi(x)$ at position x for arbitrary, statistically homogeneous two-phase random media in any spatial dimension. The local volume fraction $\xi(x)$ is defined to be the volume fraction of one of the phases, say phase 1, contained in some generally finite-sized ''observation window'' with position x. As illustrated in Fig. 1, the concentration ξ of phase 1 *within a given observation window* is a random variable ranging between 0 and 1, although the macroscopic volume fraction of phase 1 is constant, say ϕ_1. The quantity that was specifically studied by Lu and Torquato was the coarseness C, defined to be the standard deviation of ξ divided by ϕ_1.

In this paper, we study all of the moments of ξ or, equivalently, the full distribution of ξ. By generalizing the procedure of Lu and Torquato for the coarseness C, we develop a formal expression for the higher moments of ξ for statistically homogeneous and isotropic random materials. To further study local fluctuations in the volume fractions, we also consider the behavior of the *full distribution* of ξ for several models of random media using analytical and simulation methods. Assuming that the observation window has a free parameter denoted by L (for example, the side length for square observation windows), the cumulative distribution function of ξ is given by

$$F_L(x) = \Pr(\xi_L \leqslant x), \tag{1}$$

where we explicitly show the dependence of ξ on the parameter L. Notice that F_L will contain a discrete component as well as a continuous component: there is a nonzero probability that the window will be completely empty, completely covered by particles, and contain some finite number of nonoverlapping particles.

Our primary result is that, for sufficiently large observation windows (quantified below), the distribution of ξ can be reasonably approximated by a normal distribution, whose density function is given by

$$f(x) = \frac{1}{\sqrt{2\pi\sigma^2}} \exp\left[-\frac{(x-\mu)^2}{2\sigma^2}\right] \tag{2}$$

with mean $\mu = \phi_1$ and variance σ as described in Sec. III. Therefore, for large enough windows, knowledge of the first two moments is sufficient to reasonably estimate the distribution of ξ, i.e., information up to the level of the coarseness C is sufficient. This result has been rigorously proven for general ''Boolean models,'' including fully penetrable particles.[14] We will use computer simulations to establish this result for systems of impenetrable particles.

In this report we will study the distribution of the local volume fraction of five different statistically homogeneous

[a]Present address: Department of Mathematics, University of North Texas, Denton, TX 76203. E-mail: johnq@cardinal.math.unt.edu.
[b]Author to whom correspondence should be addressed. E-mail: torquato@matter.princeton.edu.

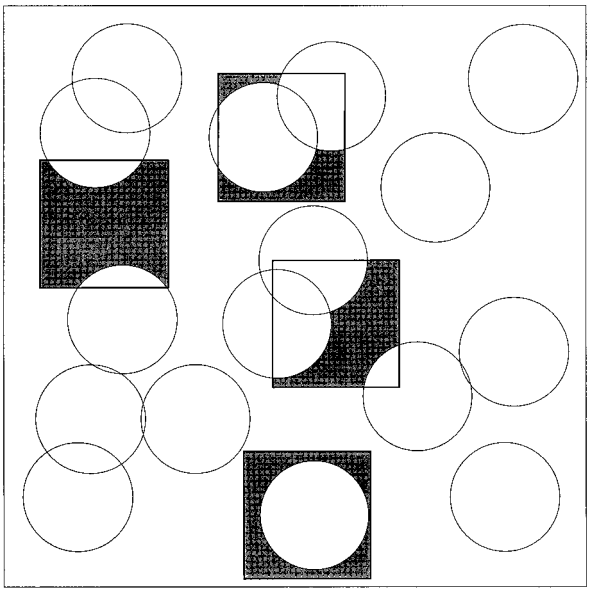

FIG. 1. A schematic depicting the local volume fraction ξ for fully penetrable disks, defined to be the fraction of an observation window which lies in phase 1 (outside the particles).

systems. On the line, we will study a system of fully penetrable rods and a system of totally impenetrable rods generated by random sequential addition (RSA). In the plane, we will study fully penetrable aligned squares and RSA totally impenetrable disks. In three dimensions, we will study fully penetrable aligned cubes. For each of these five systems, we will study computer simulations of the distribution function F_L. In the case of fully penetrable rods, we will also simplify and numerically invert a prior analytical result for the Laplace transform of F_L. We will show that, for sufficiently large window sizes, F_L can be reasonably approximated by the normal distribution for all of these models.

In Sec. II we will formally define the local volume fraction ξ and the n-point phase probability function S_n. In Sec. III we prove a general expression for the nth moment of ξ in terms of an integral over S_n. In Sec. IV we describe our method of simulating ξ for the five systems considered in this paper. In Sec. V we discuss our results for the one-dimensional systems, in Sec. VI we discuss our two-dimensional results, and in Sec. VII we discuss our three-dimensional results.

II. DEFINITIONS OF MICROSTRUCTURE FUNCTIONS

As discussed above, the local volume fraction is a measure of the microstructure of random materials on a spatially local level. Another measure of the microstructure is the n-point phase probability function S_n, which is the probability of finding n points simultaneously in phase 1. The S_n are formally defined by

$$S_n(x_1,\ldots,x_n)=\left\langle \prod_{i=1}^{n} I(x_i) \right\rangle, \tag{3}$$

where

$$I(x)=\begin{cases}1, & x \text{ in phase 1,}\\ 0, & \text{otherwise}\end{cases} \tag{4}$$

is the indicator function of phase 1. The angular brackets above denote an ensemble average over the possible realizations of the material. If the material is statistically homogeneous, then the S_n are translationally invariant and therefore are a function of the relative displacements; that is, $S_n(x_1,\ldots,x_n)=S_n(x_{12},\ldots,x_{1n})$, where $x_{1i}=x_i-x_1$. For example,

$$S_1(x_1)=\phi_1, \tag{5}$$

the volume fraction of phase 1, and

$$S_2(x_1,x_2)=S_2(x_{12}). \tag{6}$$

Under the additional assumption that the material is isotropic (i.e., directionally invariant), S_2 is dependent only on the distance between x_1 and x_2. Throughout this paper, we will restrict ourselves to statistically homogeneous and isotropic random materials.

For fully penetrable d-dimensional spheres,

$$S_n(x_1,\ldots,x_n)=\exp[-\rho V_n(x_1,\ldots,x_n)], \tag{7}$$

where ρ is the number density of the spheres and $V_n(x_1,\ldots,x_n)$ is the union volume of n spheres with radius R centered at $x_1,\ldots,x_n$. For $n=1$, this general expression simplifies to

$$\phi_1=S_1=e^{-\eta}, \tag{8}$$

where

$$\eta=\rho V_1 \tag{9}$$

is the reduced density and V_1 is the volume of a d-dimensional sphere.

As discussed in the introduction, while the volume fraction is macroscopically constant, it fluctuates on a local level. To quantify the local volume fraction, we first define a typical ''observation window'' $\mathscr{V}_x$ by

$$\mathscr{V}_x=x+\mathscr{V}_0, \tag{10}$$

where $\mathscr{V}_0$ is a base observation window containing the origin. We call x the location of V_x. The local volume fraction is then defined by[13]

$$\xi(x)=\frac{1}{V_0}\int I(z)\,\theta(z;x)\,dz, \tag{11}$$

where V_0 is the volume of $\mathscr{V}_x$ and

$$\theta(z;x)=\begin{cases}1, & z\in\mathscr{V}_x,\\ 0, & \text{otherwise}\end{cases} \tag{12}$$

is its indicator function. We notice that

$$\theta(z;x)=\theta(z-x;0)\equiv\theta(z-x) \tag{13}$$

from Eqs. (10) and (12). In the limit of a very small observation window, ξ simply becomes the phase 1 indicator function I. On the other hand, as the window becomes very large, ξ will approach the constant value ϕ_1. The simulations

of Secs. V and VI will show that ξ obeys a central limit theorem for large observation windows.

III. MOMENTS OF THE LOCAL VOLUME FRACTION

We now use the above definitions to calculate, for any n, the nth moment of the local volume fraction ξ for statistically homogeneous and isotropic random materials. We do this by relating $\langle \xi^n \rangle$ to an integral involving S_n. We also explicitly calculate the third moment of ξ for fully penetrable rods using this expression. However, this expression becomes rather difficult to calculate as n increases.

A. General result for $\langle \xi^n \rangle$

From (11), the nth moment of $\xi(x)$ is

$$\langle \xi^n(x) \rangle = \frac{1}{V_0^n} \left\langle \int I(x_1) \dots I(x_n)\, \theta(x_1;x) \dots \theta(x_n;x) \times dx_1 \dots dx_n \right\rangle$$
$$= \frac{1}{V_0^n} \int S_n(x_1, \dots, x_n)\, \theta(x_1) \dots \theta(x_n)\, dx_1 \dots dx_n, \tag{14}$$

where we have used statistical homogeneity and the fact that the observation windows are deterministic. We now use statistical homogeneity again to isolate x_1:

$$\langle \xi^n(x) \rangle = \frac{1}{V_0^n} \int S_n(0, x_2 - x_1, \dots, x_n - x_1) \times \theta(x_1) \dots \theta(x_n)\, dx_1 \dots dx_n$$
$$= \frac{1}{V_0^n} \int S_n(0, x_{12}, \dots, x_{1n}) \times \theta(x_1)\, \theta(x_1 + x_{12}) \dots \theta(x_1 + x_{1n}) \times dx_1 dx_{12} \dots dx_{1n}. \tag{15}$$

By isotropy,

$$S_n(0, x_{12}, \dots, x_{1n}) = S_n(0, -x_{12}, \dots, -x_{1n}), \tag{16}$$

since these two configurations of n points can be transformed to each other by a rotation. We finally conclude, by using a change of variables and integrating over x_1, that

$$\langle \xi^n(x) \rangle = \frac{1}{V_0^n} \int S_n(0, -x_{12}, \dots, -x_{1n})\, \theta(x_1)\, \theta(x_1 + x_{12}) \dots \theta(x_1 + x_{1n})\, dx_1 dx_{12} \dots dx_{1n}$$
$$= \frac{1}{V_0^n} \int S_n(0, x_{12}, \dots, x_{1n})\, \theta(x_1)\, \theta(x_1 - x_{12}) \dots \theta(x_1 - x_{1n})\, dx_1 dx_{12} \dots dx_{1n}$$
$$= \frac{1}{V_0^n} \int S_n(0, x_{12}, \dots, x_{1n})\, \theta(x_1; 0)\, \theta(x_1; x_{12}) \dots \theta(x_1; x_{1n})\, dx_1 dx_{12} \dots dx_{1n}$$
$$= \frac{1}{V_0^n} \int S_n(0, x_{12}, \dots, x_{1n})\, V_n^{\text{int}}(0, x_{12}, \dots, x_{1n})\, dx_{12} \dots dx_{1n}, \tag{17}$$

where $V_n^{\text{int}}(0, x_{12}, \dots, x_{1n})$ is the *intersection* volume of n observation windows with locations $0, x_{12}, \dots, x_{1n}$. We have therefore related $\langle \xi^n \rangle$ to the microstructure function S_n and the geometric intersection of n observation windows.

B. Evaluation and discussion

For $n = 1$, we obtain

$$\langle \xi \rangle = \phi_1 \tag{18}$$

from Eq. (11), and so the average of the local volume fraction is equal to the macroscopic volume fraction, as expected. To obtain the variance of ξ, we substitute $n = 2$ into Eq. (17) to obtain

$$\sigma_\xi^2 = \langle \xi^2 \rangle - \langle \xi \rangle^2 = \frac{1}{V_0^2} \int [S_2(x) - \phi_1^2] V_2^{\text{int}}(x)\, dx, \tag{19}$$

where

$$V_2^{\text{int}}(x) = \int \theta(z;0)\, \theta(z;x)\, dz \tag{20}$$

is the intersection volume of two observation windows separated by the displacement x. This is simply related to the

expression for the coarseness C that was obtained by Lu and Torquato for statistically homogeneous but possibly anisotropic media.[13] This expression for the variance of ξ is valid for this more general class of materials because Eq. (16) can be obtained from statistical homogeneity when $n=2$, and hence isotropy is not needed in the derivation of Eq. (17) for this special case.

In principle, Eq. (17) can be evaluated to obtain the higher moments of ξ. For example, for fully penetrable spheres with unit diameter and number density ρ, we can use the expression (7) for S_n to obtain the third moment of ξ for fully penetrable rods of unit length for an observation window of length L:

$$\frac{L^3\eta^3\langle\xi^3\rangle}{6}=\begin{cases}\phi_1 e^{-\eta L}(2+\eta L)+\phi_1(\eta L-2), & L<1,\\ \phi_1 e^{-\eta L}(4-\eta[2-L])+\phi_1(\eta L-2)\\ \quad+\phi_1^2(\eta^2[L-1]^2-4\eta[L-1]+6), & 1\leqslant L<2,\\ \phi_1(\eta L-2)+\phi_1^2(\eta^2[L-1]^2-4\eta[L-1]+6)\\ \quad+\phi_1^3\left(\frac{1}{6}[L-2]^3\eta^3-[L-2]^2\eta^2+3[L-2]\eta-4\right), & L\geqslant 2.\end{cases} \tag{21}$$

Unfortunately, obtaining the higher moments of ξ from Eq. (17) becomes progressively more difficult to evaluate either analytically or numerically as n increases. Therefore, to further study the nature of the local volume fraction, we will simulate the full distribution function F_L of ξ for various systems.

IV. SIMULATION PROCEDURE

Obtaining microstructural information (in this case, the local volume fraction) from computer simulations is a two-step process. First, a large number of realizations of the random material is constructed. Second, each of these realizations is sampled for the desired microstructure function. In many cases, these sample data are averaged to obtain the microstructure function in question. To study the behavior of the F_L, however, we will need to examine the full sample cumulative distribution function of the sample local volume fractions. By exactly determining the sample local volume fractions, we eliminate the uncertainties inherent with Monte Carlo measurement for this stage of the simulation. We also preserve the discontinuities in the cumulative distribution function of the local volume fraction.

For the one-dimensional systems studied in this report, namely fully penetrable rods and RSA totally impenetrable rods, we generated systems of 10^6 rods at different volume fractions. Periodic boundary conditions were employed. To calculate efficiently a large number of sample ξ, we then considered a large number of windows whose left endpoints formed an arithmetic sequence with span less than the length of a single rod. The fraction of each window that belongs to the void phase is then exactly calculated. By studying these windows from left to right, we rapidly calculated the volume fraction of phase 1 of one window by using the measured data for the previous window. Finally, the sample local volume fractions are then placed into a large (say 5000) number of bins on the interval [0,1]. The sample cumulative distribution functions were then easily obtained from this binned data.

We proceed similarly in higher dimension. For the two-dimensional systems of fully penetrable aligned squares and RSA totally impenetrable circles, we generated systems of 10^6 particles at different volume fractions, again employing periodic boundary conditions. For the three-dimensional system of fully penetrable cubes, 400 000 particles were used. The observation windows chosen for these systems were randomly placed squares (cubes in three dimensions) of known length. The fraction of the window belonging to the void phase was again exactly determined for any given window. Finally, these sample local volume fractions were binned to produce the sample distribution functions.

V. RESULTS AND DISCUSSION: ONE-DIMENSIONAL SYSTEMS

In this section we use computer simulations to study the behavior of the distribution of ξ for fully penetrable rods and for RSA hard rods. For fully penetrable rods, we also numerically invert a previous analytical expression for the Laplace transform of the F_L. For both systems, we measure how well a normal distribution fits F_L for different values of the window length and the volume fraction of the particle phase.

A. Fully penetrable rods

In our first model, we consider a system of equal-sized fully penetrable rods. To construct such a system, we take a Poisson process on the line with some given density η and center on each of the points a rod with unit length. For this system, the volume fraction of phase 1 is given by Eq. (8), and the two-point phase probability function is

$$S_2(x)=\begin{cases}\phi_1 e^{-\eta|x|}, & |x|<1,\\ \phi_1^2, & \text{otherwise.}\end{cases} \tag{22}$$

Therefore, from Eq. (19), the variance of the local volume fraction of phase 1 in an interval of length L is

$$\sigma_\xi^2 = 2\phi_1^2 \int_0^{\min(L,1)} [e^{\eta(1-x)} - 1](L-x)dx, \tag{23}$$

which can be simplified as

$$\sigma_\xi^2 = \begin{cases} \dfrac{1}{\eta L}\sqrt{2\phi_1(\eta L + \exp[-\eta L] - 1) - \phi_1^2\eta^2 L^2}, & L < 1, \\ \dfrac{1}{\eta L}\sqrt{2\phi_1(1-\eta L)(\phi_1 + \eta\phi_1 - 1) + \eta^2\phi_1^2}, & L \geqslant 1. \end{cases} \tag{24}$$

The third moment of ξ for this system was given in Eq. (21).

As discussed above, the mean and variance can be inserted into Eq. (2) to obtain an asymptotic approximation of the distribution function F_L of ξ for large L.

1. Laplace transform of local volume fraction distribution

Some analytical results for the distribution of ξ away from the asymptotic limit have been obtained for fully penetrable rods, unlike the other models considered in this report. For example, if the window size L is less than the length of a rod, then it is known that[14]

$$\Pr(\xi = 0) = 1 - (1 + \eta L)\phi_1, \tag{25}$$

$$\Pr(\xi = L) = \phi_1 e^{-\eta L}, \tag{26}$$

and

$$\Pr(\xi \in dx | 0 < \xi < L) = \frac{\eta[2 + \eta(L-x)]e^{\eta(L-x)}}{(1+\eta x)e^{\eta x} - 1}dx. \tag{27}$$

However, except for this special case, obtaining the distribution of ξ analytically is a difficult exercise.

Domb[15] studied the cumulative distribution function T of the length x of the rod phase in an observation window of length L, so that

$$T(x,L) = 1 - F_L(1 - x/L) \tag{28}$$

where $0 \leqslant x \leqslant L$. He showed that the discontinuities of T have magnitude

$$T^+(k,L) - T^-(k,L) = \frac{\eta^k (L-k)^k}{k!} e^{-\eta(L+1)} \tag{29}$$

at $x = n < L$ for integer n, and

$$1 - T^-(L,L) = 1 + \sum_{k=1}^{m} (-1)^k \phi_1^k \left(\frac{[\eta(L-k+1)]^{k-1}}{(k-1)!} + \frac{[\eta(L-k+1)]^k}{k!} \right), \tag{30}$$

where m is the positive integer which satisfies $m - 1 \leqslant L < m$. This last quantity is also the two-point cluster function for fully penetrable rods.[16]

Domb also calculated the Laplace transform (albeit an unconventional definition of the Laplace transform) of the derivative of T for $x < L$. Clearly $T(L,L) = 1$, and so we will ignore this special case in the following. Using Domb's result, the Laplace transform of $T(x,L)$ with respect to x is

$$\begin{aligned} \hat{T}(x,L) &= \int_0^\infty e^{-sx} T(x,L)dx \\ &= \frac{1}{s}\sum_{r=0}^{\infty} \sum_{n=0}^{r} \binom{r}{n} L^{r-n} \frac{d^n}{ds^n} \\ &\quad \times \left[\frac{[B(s) - \eta]^r}{r!} \frac{A(s) + B(s)C(s)}{s} \right], \end{aligned} \tag{31}$$

where

$$A(s) = \frac{\phi_1(s+\eta)(s+\eta-\eta e^{-s})}{s + \eta\phi_1 e^{-s}}, \tag{32}$$

$$B(s) = \frac{\eta\phi_1(s+\eta)e^{-s}}{s + \eta\phi_1 e^{-s}}, \tag{33}$$

and

$$C(s) = \frac{s(1-\phi_1) - \eta\phi_1(1-e^{-s})}{s + \eta\phi_1 e^{-s}}. \tag{34}$$

Equation (31) can be simplified using complex analysis. We first notice that

$$\begin{aligned} \hat{T}(x,L) &= \frac{1}{s}\sum_{n=0}^{\infty} \sum_{t=0}^{\infty} \frac{L^t}{n!t!} \frac{d^n}{ds^n} \\ &\quad \times \left[\{B(s) - \eta\}^{n+t} \frac{A(s) + B(s)C(s)}{s} \right] \\ &= \frac{1}{s}\sum_{n=0}^{\infty} \frac{1}{n!} \frac{d^n}{ds^n} \left[\{B(s) - \eta\}^n \right. \\ &\quad \left. \times \exp\{L[B(s) - \eta]\} \frac{A(s) + B(s)C(s)}{s} \right]. \end{aligned} \tag{35}$$

Using Cauchy's integral formula,[17] this can be transformed to

$$\hat{T}(x,L)=\frac{1}{2\pi s i}\sum_{n=0}^{\infty}\int_{\Gamma}\frac{[B(z)-\eta]^n\,\exp\{L[B(z)-\eta]\}[A(z)+B(z)C(z)]}{z(z-s)^{n+1}}dz, \tag{36}$$

where Γ is any closed curve containing s such that

$$z+\eta\phi_1 e^{-z}\neq 0 \tag{37}$$

for all z in the region enclosed by Γ. This condition is needed to ensure that the integrand contains no poles within Γ.

The sum and integral can be interchanged if the sum on n converges. This will occur whenever

$$|B(z)-\eta|<|z-s| \quad \text{for all } z \text{ on } \Gamma. \tag{38}$$

From our experience, this condition will fail at all reduced densities η for sufficiently large observation windows. That is, at any η, no curve Γ can be drawn which simultaneously satisfies Eqs. (37) and (38) for all $x<L$.

Nevertheless, under these assumptions, the Laplace transform of T finally reduces to

$$\hat{T}(x,L)=\frac{\phi_1}{2\pi i}\int_{\Gamma}\frac{(z+\eta)^2\,\exp\{y[B(z)-\eta]\}}{s[z-s-B(z)+\eta](z+\eta\phi_1 e^{-z})^2}dz. \tag{39}$$

Recall that

$$B(z)-\eta=-\frac{\eta z(1-\phi_1 e^{-z})}{z+\eta\phi_1 e^{-z}}. \tag{40}$$

In summary, under the assumptions (37) and (38), we have analytically represented the Laplace transform of F_L as a single integral in the complex plane.

In order to obtain F_L from Eq. (39), we will use two different short algorithms discovered by Abate and Whitt, using the Fourier-series method,[18,19] which numerically calculate any function g from its Laplace transform $\hat{g}$. These algorithms require that $|g(t)|<1$ and that $\hat{g}(s)$ can be evaluated at any point s in the complex plane. (These authors have also developed numerical techniques for inverting Laplace transforms of other functions.[18]) In our case, F_L is a cumulative probability function, and since we have an explicit formula for its transform via Eqs. (28) and (39), we can use their numerical methods to numerically obtain F_L.

These algorithms unfortunately do not have simple general error bounds. To ensure numerical accuracy, Abate and Whitt suggest that the two methods be used separately and checked for agreement within desired precision. In our case, we have a third method of checking the computation of the local volume fraction, namely, direct Monte Carlo simulation.

The authors recommend that the Laplace transform be evaluated to double floating point precision. In our case, the transform is an integral, and evaluating it to that degree of precision can be computationally intensive. Our experience is that evaluating $\hat{T}$ to 10 or 11 decimal places yields values of T accurate to 3 or 4 decimal places.

Finally, by using this algorithm, we can measure at which values of L the assumption (38) will fail. Fortunately, as we shall see, the asymptotic normal approximation can be accurately used in this domain.

2. Results for fully penetrable rods

In Fig. 2 we plot the probability density function, obtained from simulations, for ξ for fully penetrable rods and a

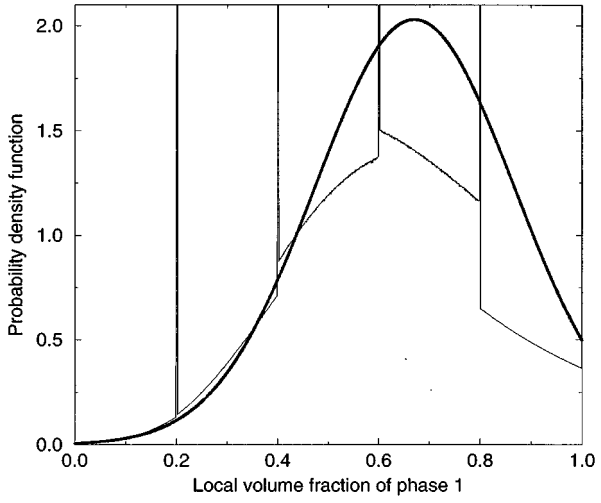

FIG. 2. The probability density function of ξ with $L=5$ for a system of fully penetrable rods with $\eta=0.4$, and a normal distribution with parameters given by Eqs. (8) and (24). We see that there are ''spikes'' in the density function corresponding to having no, one, two, three, and four nonoverlapping rods within the window, and to having the window completely covered by rods.

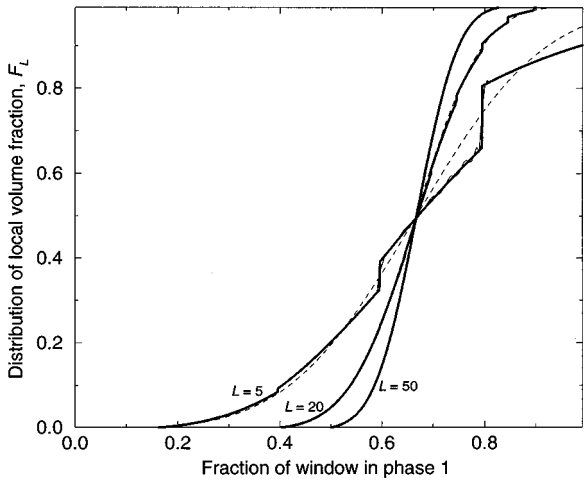

FIG. 3. The distribution function of ξ for a system of fully penetrable rods with reduced density $\eta=0.4$. The windows are intervals with lengths $L=5$, $L=20$ and $L=50$. The thick solid lines are simulation data, the thin solid lines are values obtained from numerically inverting the Laplace transform of ξ, and the dashed lines are normal approximations.

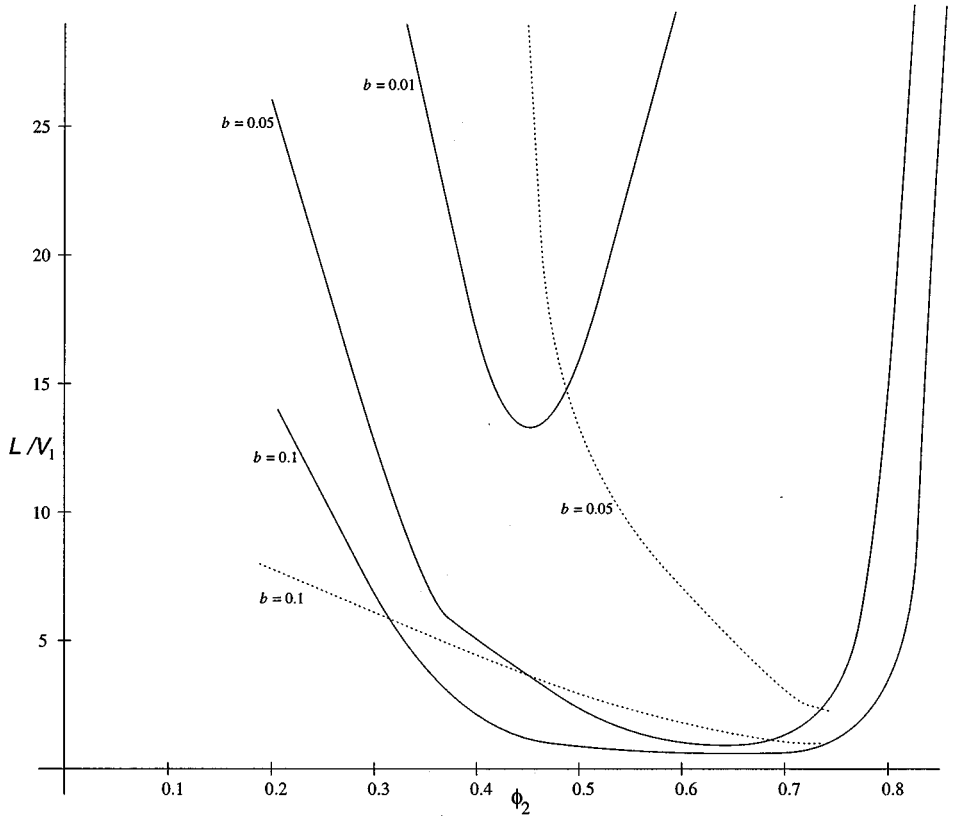

FIG. 4. Level curves of the maximum separation b, defined by Eq. (42). The x-axis is the particle volume fraction $\phi_2=1-\phi_1$, and the y-axis is the ratio of the observation window length and the particle length V_1. Level curves of b are shown for fully penetrable rods (solid lines) and RSA totally impenetrable rods (dotted lines). The level curves for b for fully penetrable rods are $b=0.1$, $b=0.05$ and $b=0.01$. For RSA totally impenetrable rods, the levels curves are $b=0.1$ and $b=0.05$; the level curve for $b=0.01$ is not on the scale of this figure.

normal distribution. The system parameters for Fig. 2 are $\eta=0.4$ and $L=5$, and the moments of the normal distribution are determined by Eqs. (8) and (24). As expected, there are ''spikes'' in the density function at $x=0,1/5,\ldots,1$, since there are positive probabilities, given by Eqs. (29) and (30), that a given observation window will lie entirely in phase 1, phase 2, or contain some number of nonoverlapping rods. We also observe that, while ξ has domain $[0,1]$, the normal distribution is defined on the entire real line. We will show, however, that these distinctions diminish as the size of the observation window increases.

In Fig. 3 we show the cumulative distribution function F_L of ξ obtained from computer simulations and by numerical inversion at three different observation window lengths; these are compared with normal distribution function Φ, defined by

$$\Phi(x)=\int_{-\infty}^{x} f(t)dt, \tag{41}$$

where the normal density function f was defined by (2), with parameters determined by Eqs. (8) and (24). For these systems, we choose systems of fully penetrable rods with $\eta=0.4$. The discontinuities in the graphs of the F_L have magnitudes given by Eqs. (29) and (30).

We see that the numerical inversions of Eq. (39) contain oscillations. This is not a surprising result: the inversion method is based on a Fourier-series expansion, but the distribution of F_L contains points of discontinuity. Therefore, we are witnessing the Gibbs effect when a discontinuous function is approximated by a Fourier series. As the magnitudes of the discontinuities decrease (that is, for large L), so do the oscillations. Although we do not use them here, more computationally intensive techniques have been developed to invert the Laplace transforms of discontinuous functions without oscillations.[20]

We also see in Fig. 3 that the graphs of F_L approach the normal distribution as L increases: while the graph of F_5 is clearly not normal, the graph of F_{50} cannot be distinguished from a normal distribution on the scale of this figure. To quantitatively assess how close the F_L are to a normal distribution, we measure the *maximum separation* between the sample distribution and the normal distribution, that is,

$$b=\max_{x\in[0,1]}[F_L(x)-\Phi(x)]. \tag{42}$$

Clearly the separation b is dependent on the particle volume fraction ϕ_2, which is

$$\phi_2=1-e^{-\eta} \tag{43}$$

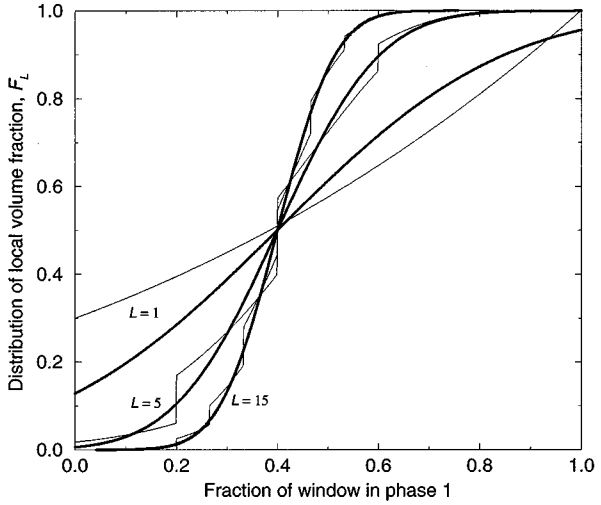

FIG. 5. The normal distribution (thick line) and simulation graphs of the local volume fraction of RSA hard rods at $\eta=0.4$. The windows have lengths $L=1$, $L=5$ and $L=15$. We see that the normal curve becomes a more reasonable approximation to F_L as L increases.

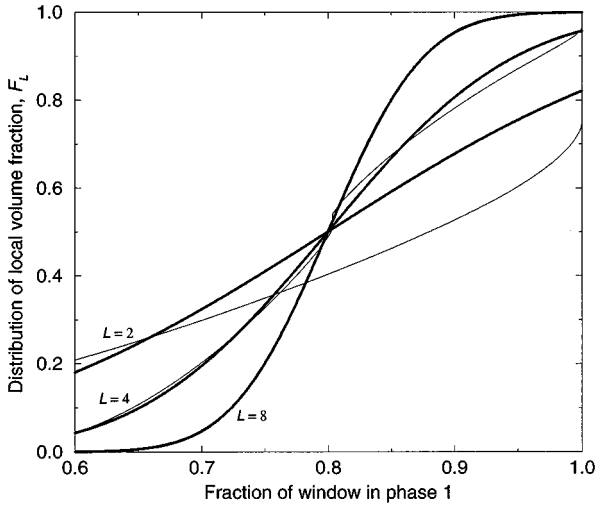

FIG. 6. The distribution of the local volume fraction of RSA totally impenetrable disks at $\eta=0.2$. The F_L converge much more quickly to a normal distribution in two dimensions.

for fully penetrable rods, and the window length L. In Fig. 4 we present approximate level curves of b (i.e., curves in the ϕ_2–L/V_1 plane on which b is constant, where V_1 is the length of a single rod). These level curves are obtained from computer simulation data and hence should not be regarded as precisely correct. However, we believe that these level curves can be used to approximately measure how close F_L is to a normal distribution for a given system of fully penetrable rods. Based on empirical evidence, the sample distributions are extremely close to the normal distribution when $b\leqslant 0.02$. As reflected in Fig. 4, this occurs for fully penetrable rods for $L/V_1\geqslant 20$ when $\phi_2=0.3$, but is satisfied for $L\geqslant 5$ for $\phi_2=0.6$.

In summary, for sufficiently large windows, the distribution of ξ can be reasonably approximated by a normal distribution. For smaller windows, the numerical techniques described above can be used to obtain F_L.

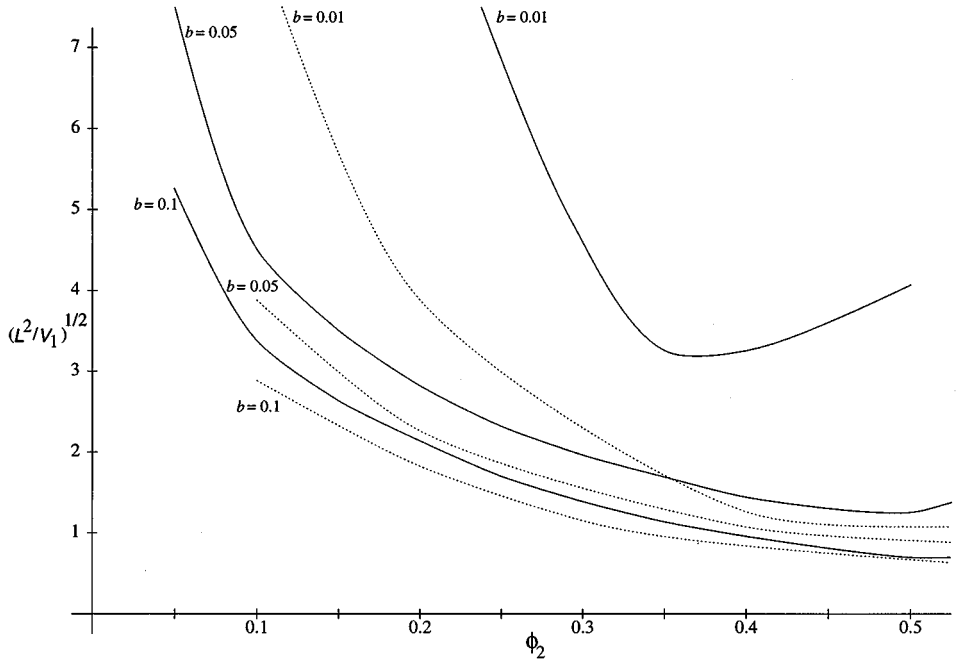

FIG. 7. As in Fig. 4, except for the two-dimensional systems of fully penetrable squares (solid lines) and RSA totally impenetrable disks (dotted lines). The y-axis is the square root of the ratio of the area of the observation window to V_1, the area of a single particle. The level curves are $b=0.1$, $b=0.05$ and $b=0.01$ for both systems.

B. Totally impenetrable rods

The second model considered in this report is a system of totally impenetrable rods generated by random sequential addition. To generate such a system, particles are randomly added in sequence so that they do not overlap and are ''parked'' into their positions for all time. Unlike the previous model, there is a ''jamming limit'' (i.e., a maximum possible η) at which point no additional particles can be introduced into the system. This jamming limit is known analytically in one dimension and is given by[21]

$$\eta^c = \int_0^\infty \exp\left[-2 \int_0^t \left(\frac{1-e^{-s}}{s} \right) ds \right] dt \approx 0.7476. \tag{44}$$

We again will obtain graphs of the distribution of ξ by computer simulations and show that, for sufficiently large window sizes, they can be reasonably approximated by a normal distribution.

In Fig. 5 we have plotted a normal distribution and the sample distributions of ξ for $L=1$, $L=5$ and $L=15$ for a system of RSA hard rods at $\eta=\phi_2=0.4$. The normal distributions were computed using the theoretical mean $\mu=\eta$ and the sample coarseness C. Recently, the radial distribution function for RSA hard rods has been found analytically.[22] Using this result, the function S_2 can in principle be obtained,[23] and so the standard deviation can be obtained theoretically from Eq. (19). However, this calculation is exceptionally tedious, and so we instead use the sample coarseness C.

We see that, just as with systems of fully penetrable rods, there is a discrete as well as a continuous component to the graphs of the F_L. We also see that a normal distribution provides a reasonable approximation to F_L as L increases. However, the convergence to a normal does not appear to be as fast as with fully penetrable rods. This is not surprising: for large L, the probability that some number of nonoverlapping particles will lie in a given observation window will be roughly $\phi_1^2>0$, and so the sum of the discontinuities of F_L will be strictly positive for any L. This is in contrast to the case of fully penetrable rods, where the sum of the discontinuities tends to zero [from Eqs. (29) and (30)] as L tends to infinity.

We have also plotted level curves for the maximum separation between F_L and the normal distribution Φ for RSA totally impenetrable rods in Fig. 4. We see that, at the same ϕ_2 and L, the distribution of ξ for fully penetrable rods is closer to normal than for RSA hard rods. As we will see in the next section, however, this behavior is an artifact of the specific geometry on the line.

VI. RESULTS AND DISCUSSION: TWO-DIMENSIONAL SYSTEMS

We now study the behavior of the F_L for RSA hard disks and for fully penetrable squares. We find that the rate of convergence to a normal distribution is much faster than for the one-dimensional models of the previous section.

A. Totally impenetrable disks

We now consider a two-dimensional system of RSA totally impenetrable disks with unit radius. Since the particles are not permitted to overlap, there is also a jamming limit for this model. This jamming limit is unknown theoretically, but from computer simulations[24,25] its value is known to be approximately $\eta^c \approx 0.55$.

In Fig. 6 we plot normal distributions and the F_L for this model at $\eta=0.2$ for $L=2$, $L=4$ and $L=8$. Once again, since S_2 is unknown theoretically except in terms of the radial distribution function,[23] the normal distributions are determined by the theoretical mean $\mu=\eta$ and sample coarseness C. We see that the convergence to a normal distribution is much quicker than in one dimension.

In Fig. 7 we plot level curves of the maximum separation, defined by Eq. (42), for the two-dimensional systems considered in this report. These level curves are plotted on the $\phi_2-(L^2/V_1)^{1/2}$ plane, where ϕ_2 again is the particle volume fraction, L is the side length of the observation window, and V_1 is the area of a single particle. For totally impenetrable disks of unit radius, $\phi_2=\eta$ and $V_1=\pi$. We again notice that the convergence is faster in two dimensions than in one. We also observe that the convergence of F_L for RSA disks is quicker than for fully penetrable squares, discussed in the next section. This is not surprising, since the variance of ξ for totally impenetrable particles is less than the variance for fully penetrable particles.[13] Again, a reasonable empirical condition for closeness to a normal distribution appears to be $b \leqslant 0.02$. As seen in Fig. 7, this occurs for RSA totally impenetrable disks for $(L^2/V_1)^{1/2} \geqslant 7$ (i.e., $L \geqslant 12.4$, where again the particles have unit radius) when $\phi_2=0.1$, but for $L \geqslant 3$ when $\phi_2=0.4$.

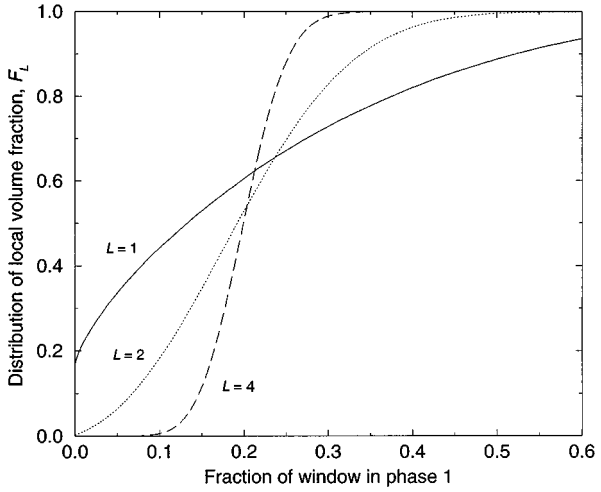

FIG. 8. The distribution of the local volume fraction of fully penetrable aligned cubes at $\phi_2=0.20$. The F_L converge even more rapidly in three dimensions.

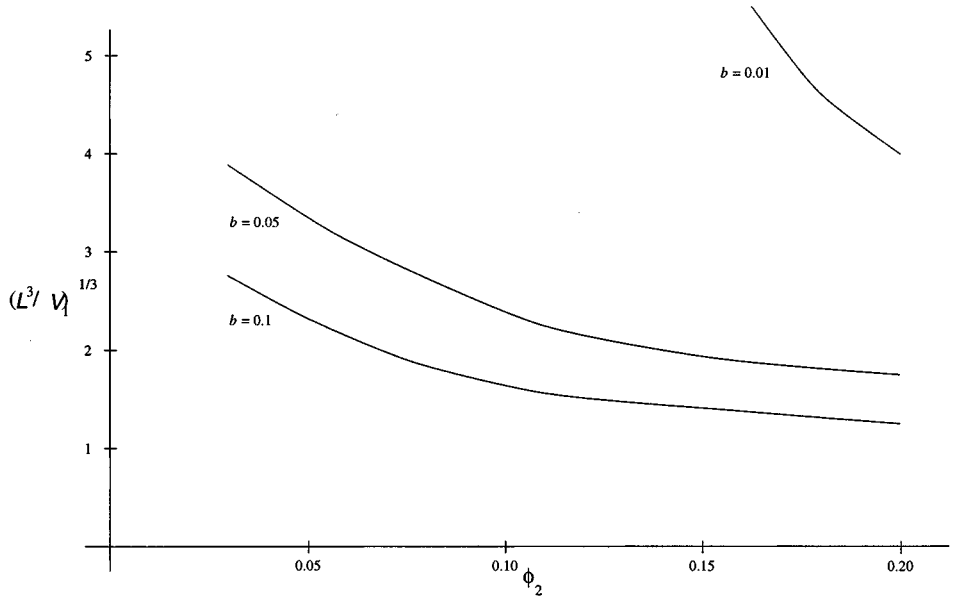

FIG. 9. As in Fig. 4, except for the fully penetrable aligned cubes. The y-axis is the ratio of the window side length to the particle side length. The level curves are $b=0.1$, $b=0.05$ and $b=0.01$.

B. Fully penetrable aligned squares

Another two-dimensional model is a system of fully penetrable aligned squares with density η and unit side length. We take a square window of side length L aligned with the particles. The spatial central limit theorem can be applied to this model, and so we know theoretically that the distribution functions F_L are asymptotically normal. For this system,

$$\mu \equiv \phi_1 = e^{-\eta} \tag{45}$$

and

$$S_2(x,y) = \begin{cases} \phi_1^2 \exp[\eta(1-|x|)(1-|y|)], & |x|,|y|<1, \\ \phi_1^2, & \text{otherwise.} \end{cases} \tag{46}$$

Substituting into Eq. (19), we find that

$$\sigma_\xi^2 = \frac{4\phi_1^2}{L^4}\int_0^{\min(L,1)}\int_0^{\min(L,1)} [\exp\{\eta(1-x)(1-y)\}-1] \times (L-x)(L-y)\,dx\,dy, \tag{47}$$

which simplifies as

$$\sigma_\xi^2 = \frac{\phi_1^2}{\eta^2 L^4}(-\eta^2 L^4 - 4e^{\eta} + 8e^{\eta(1-L)} - 4e^{\eta(1-L)^2} + 8e^{\eta} L - 8e^{\eta(1-L)}L - 4[\,\mathrm{Ei}(\eta) - 2\,\mathrm{Ei}(\eta\{1-L\}) + \mathrm{Ei}(\eta\{1-L\}^2)](1-\eta+2\eta L-\eta L^2)) \tag{48}$$

for $L<1$, while

$$\sigma_\xi^2 = -\frac{\phi_1^2(2L-1)^2}{L^4} + \frac{4}{L^4}\Bigg([-1+\eta-2\eta L + \eta L^2]\frac{\phi_1^2\,\mathrm{Ei}(\eta)}{\eta^2} + \frac{(1-L)\phi_1^2[2+(L-1)(\ln\eta+\gamma)]}{\eta} + \frac{\phi_1[-1+2L+(1+\gamma)\phi_1-2\phi_1 L+\phi_1\ln\eta]}{\eta^2}\Bigg) \tag{49}$$

for $L>1$. In these expressions

$$\mathrm{Ei}(x) = \int_{-\infty}^{x}\frac{e^t}{t}dt \tag{50}$$

is the exponential integral function for $x>0$, and γ is Euler's constant.

Level curves of the maximum separation of the F_L are shown in Fig. 7. For fully penetrable aligned squares with unit side length, $\phi_2 = 1-e^{-\eta}$ and $V_1=1$. We notice that, as with the coarseness, the maximum separation is smaller for totally impenetrable particles than for penetrable particles. In other words, to obtain the same maximum separation at the same volume fraction, the window size for fully penetrable squares is somewhat larger than the window size for RSA totally impenetrable disks.

VII. RESULTS AND DISCUSSION: THREE-DIMENSIONAL SYSTEMS

The final model considered in this report is a system of fully penetrable aligned cubes with density η and unit side length. (We do not present simulations of RSA spheres here; this simulation would require knowledge of the intersection of a cubical window with a spherical particle, which cannot be expressed in closed form.) We take a cubical window of side length L aligned with the particles. The spatial central limit theorem can be applied to this model, and so we know theoretically that the distribution functions F_L are asymptotically normal. We find that

$$\mu \equiv \phi_1 = e^{-\eta} \tag{51}$$

and

$$\sigma_\xi^2 = \frac{8\phi_1^2}{L^6}\int_0^{\min(L,1)}\int_0^{\min(L,1)}\int_0^{\min(L,1)} [\exp\{\eta(1-x)(1-y)(1-z)\}-1](L-x)(L-y)(L-z)\,dx\,dy\,dz. \tag{52}$$

Unfortunately, this triple integral for the variance of ξ cannot be evaluated in closed form.

Our simulated distribution functions F_L are shown in Fig. 8 for $\phi_2 = 0.20$. Level curves of the maximum separation of the F_L are shown in Fig. 9. For fully penetrable aligned cubes with unit side length, $\phi_2 = 1 - e^{-\eta}$ and $V_1 = 1$. We notice that a somewhat smaller ratio of window side length to particle side length is required in order to obtain the same maximum separation b.

VIII. CONCLUSIONS

We have developed a formal analytical expression for arbitrary moments of the local volume fraction, and we have used analytical and computer-simulation methods to study the full distribution of the local volume fraction for five different models of random media. We have seen that, for all of these models, the distribution numerically tends to a normal distribution as the size of the window increases and hence the standard deviation or coarseness C provides a good estimate of the fluctuations. The convergence to a normal distribution increases with the dimension of the system.

ACKNOWLEDGMENTS

The authors gratefully acknowledge the support of the Air Force Office of Scientific Research under Grant No. F49620-92-J-0501 and the U.S. Department of Energy, Office of Basic Energy Sciences under Grant No. DE-FG02-92ER14275. J.Q. was supported in part under a National Science Foundation Graduate Fellowship.

[1] S. Prager, Physica **29**, 129 (1963).
[2] M. Beran, *Statistical Continuum Theories* (Wiley, New York, 1968).
[3] G. W. Milton, Phys. Rev. Lett. **46**, 542 (1981).
[4] G. W. Milton, Commun. Math. Phys. **111**, 281 (1987).
[5] S. Torquato, Appl. Mech. Rev. **44**, 37 (1991).
[6] P. Debye, H. R. Anderson, and H. Brumberger, J. Appl. Phys. **28**, 679 (1957).
[7] S. Torquato and F. Lado, J. Chem. Phys. **94**, 4453 (1991).
[8] E. O'Neill, *Introduction to Statistical Optics* (Addison–Wesley, Reading, MA, 1963).
[9] B. E. Bayer, J. Opt. Soc. Am. **54**, 1485 (1964).
[10] B. Lu and S. Torquato, J. Opt. Soc. Am. A **7**, 717 (1990).
[11] R. S. Fishman, D. A. Kurtze, and G. P. Bierwagen, J. Appl. Phys. **72**, 3116 (1992).
[12] J. Botsis and C. Beldica, Int. J. Fracture (in press).
[13] B. Lu and S. Torquato, J. Chem. Phys. **93**, 3452 (1990).
[14] P. Hall, *Introduction to the Theory of Coverage Processes* (Wiley, New York, 1988).
[15] C. Domb, Proc. Camb. Philos. Soc. **43**, 329 (1947).
[16] E. Çinlar and S. Torquato, J. Stat. Phys. **78**, 827 (1995).
[17] L. Ahlfors, *Complex Analysis* (McGraw-Hill, New York, 1979).
[18] J. Abate and W. Whitt, Queueing Systems **10**, 5 (1992).
[19] J. Abate and W. Whitt, ORSA J. Comput. **7**, 36 (1995).
[20] L. K. Platzman, J. C. Ammons, and J. J. Bartholdi, Oper. Res. **36**, 137 (1988).
[21] B. Widom, J. Chem. Phys. **44**, 3888 (1966).
[22] B. Bonnier, D. Boyer, and P. Viot, J. Phys. A: Math. Gen. **27**, 3671 (1994).
[23] S. Torquato and F. Lado, J. Phys. A: Math. Gen. **18**, 141 (1985).
[24] J. Feder, J. Theoret. Biol. **87**, 237 (1980).
[25] M. Tanemura, Ann. Inst. Stat. Math. **31B**, 351 (1979).